farmers alone. If this is the case, then subsequent dilution through migration and admixture, after the arrival of the first farmers, would need to be invoked, implying multiple episodes of population turnover, which are not necessarily observable in the archaeological record. This, in turn, would mean that the classic model of European ancestry components (contrasting hunter-gatherers with early Neolithic farming pioneers) requires revision.

The geographic origin of the demographic processes that brought the early farmer mtDNA types to central Europe now becomes a major question. On the one hand, all of the early farmer remains analyzed here are associated with the LBK culture of central Europe. Based on ceramic typology, the LBK culture is thought to have originated in present-day western Hungary and southwestern Slovakia, with a possible predecessor in the southeast European Starçevo-Kris culture (*19*, *20*). These cultural source locations may provide the most plausible origins or routes for the geographic spread of the early farmers, considering that the LBK was the first major farming culture in central and northern Europe and is archaeologically attested to have disseminated over five centuries and covered nearly a million square kilometers. Alternatively, the farmers' mtDNA types may have an origin closer to the Neolithic core zone in southwestern Asia. Further ancient DNA analysis of early farmer samples from southeastern Europe and Anatolia will be required to resolve this question.

References and Notes

1. P. Mellars, *Nature* **432**, 461 (2004).
2. K. Harvati, in *Handbook of Paleoanthropology*, W. Henke, I. Tattersall, Eds. (Springer, Berlin, 2007), vol. 3, pp. 1717–1748.
3. T. Terberger, M. Street, *Antiquity* **76**, 691 (2002).
4. B. V. Eriksen, in *Recent Studies in the Final Palaeolithic of the European Plain*, B. V. Eriksen, B. Bratlund, Eds. (Jutland Archaeological Society, Højbjerg, Denmark, 2002), pp. 25–42.
5. G. Eberhards, I. Zagorska, in *Recent Studies in the Final Palaeolithic of the European Plain*, B. V. Eriksen, B. Bratlund, Eds. (Jutland Archaeological Society, Højbjerg, Denmark, 2002), pp. 85–90.
6. V. G. Childe, *The Dawn of European Civilization* (Kegan Paul, London, 1925).
7. M. Richards *et al.*, *Am. J. Hum. Genet.* **67**, 1251 (2000).
8. A. Achilli *et al.*, *Am. J. Hum. Genet.* **75**, 910 (2004).
9. M. Currat, L. Excoffier, *Proc. Biol. Sci.* **272**, 679 (2005).
10. G. de Mortillet, *La Formation de la Nation Française. Textes-Linguistique-Palethnologie-Anthropologie* (F. Alcan, Paris, 1897)
11. W. Haak *et al.*, *Science* **310**, 1016 (2005).
12. W. Haak, thesis, Mainz University, Mainz, Germany (2006).
13. A. Roehl, B. Brinkmann, L. Forster, P. Forster, *Int. J. Legal Med.* **115**, 29 (2001).
14. Information on materials and methods is available as supporting material on *Science* Online.
15. S. Schneider, D. Roessli, L. Excoffier, "Arlequin: A software for population genetics data analysis. Ver 2.000" (Genetics and Biometry Lab, Department of Anthropology, University of Geneva, Geneva, Switzerland, 2000).
16. A. Zimmermann, J. Richter, J, Th. Frank, P. Wendt, *Ber. Rom.-Ger.Komm.* **85**, 37 (2004).
17. R. Nielsen, M. A. Beaumont, *Mol. Ecol.* **18**, 1034 (2009).
18. D. Gronenborn, *Silexartefakte der Ältestbandkeramischen Kultur* (Universitätsforschungen zur prähistorischen Archäologie 37, Habelt, Bonn, Germany, 1997).
19. J. Pavuk, in *Die Bandkeramik im 21. Jahrhundert: Symposium in der Abtei Brauweiler bei Köln 2002*, J. Lüning, C. Frirdich, A. Zimmermann Eds. (VML Vlg Marie Leidorf, Rahden/Westfahlen, Germany, 2005), pp 17–39.
20. I. Mateiciucová, *Arch. Inf.* **26**, 299 (2003).
21. M. Zvelebil, in *Harvesting the Sea, Farming the Forest. The Emergence of Neolithic Societies in the Baltic Region*, M. Zvelebil, L. Domanska, R. Dennell, Eds. (Sheffield Academic Press, Sheffield, UK, 1998), pp. 9–27.
22. R. M. Andrews *et al.*, *Nat. Genet.* **23**, 147 (1999).
23. U. Danzeglocke, O. Jöris, B. Weninger, CalPal Online (2007) (www.calpal-online.de).

24. The authors are grateful to W. Guminski (Institute of Archeology and Ethnology, Polish Academy of Sciences, Warsaw, Poland), J. Siemaszko (Suwalki Province Museum, Suwalki, Poland), A. Khokhlov (Institute of Cell Biophysics, Russian Academy of Sciences, Pushchino, Moscow oblast, Russia), H. Meller and M. Porr (Landesamt für Archäologie Sachsen-Anhalt, Halle/Saale, Germany), and L. P. Louwe Kooijmans and L. Smits (Faculty of Archeology, Leiden University, Leiden, Netherlands) for providing them with the archaeological samples. The authors are indebted to R. Villems, A. Zimmermann, and J. Lüning for comments and to D. Kasperaviciute for Lithuanian sequences. We also thank M. Forster for editorial comments. Research grants were provided by the Bundesministerium für Bildung und Forschung, the Deutsche Forschungsgemeinschaft, and the Estonian Science Foundation (grant no. 6040 to K.T).

Supporting Online Material

www.sciencemag.org/cgi/content/full/1176869/DC1
Materials and Methods
Fig. S1
Tables S1 to S6
References

27 May 2009; accepted 21 August 2009
Published online 3 September 2009;
10.1126/science.1176869
Include this information when citing this paper.

Ribosomal Protein S6 Kinase 1 Signaling Regulates Mammalian Life Span

Colin Selman,[1]* Jennifer M. A. Tullet,[2] Daniela Wieser,[3] Elaine Irvine,[1] Steven J. Lingard,[1] Agharul I. Choudhury,[1] Marc Claret,[1] Hind Al-Qassab,[1] Danielle Carmignac,[4] Faruk Ramadani,[5] Angela Woods,[6] Iain C. A. Robinson,[4] Eugene Schuster,[3] Rachel L. Batterham,[1] Sara C. Kozma,[7] George Thomas,[7] David Carling,[6] Klaus Okkenhaug,[5] Janet M. Thornton,[3] Linda Partridge,[2] David Gems,[2] Dominic J. Withers[1,8]†

Caloric restriction (CR) protects against aging and disease, but the mechanisms by which this affects mammalian life span are unclear. We show in mice that deletion of ribosomal S6 protein kinase 1 (S6K1), a component of the nutrient-responsive mTOR (mammalian target of rapamycin) signaling pathway, led to increased life span and resistance to age-related pathologies, such as bone, immune, and motor dysfunction and loss of insulin sensitivity. Deletion of *S6K1* induced gene expression patterns similar to those seen in CR or with pharmacological activation of adenosine monophosphate (AMP)–activated protein kinase (AMPK), a conserved regulator of the metabolic response to CR. Our results demonstrate that S6K1 influences healthy mammalian life span and suggest that therapeutic manipulation of S6K1 and AMPK might mimic CR and could provide broad protection against diseases of aging.

Genetic studies in *Saccharomyces cerevisiae*, *Caenorhabditis elegans*, and *Drosophila melanogaster* implicate several mechanisms in the regulation of life span. These include the insulin and insulin-like growth factor 1 (IGF-1) signaling (IIS) pathway and the mammalian target of rapamycin (mTOR) pathway, which both activate the downstream effector ribosomal protein S6 kinase 1 (S6K1) (*1*, *2*). Although the role of these pathways in mammalian aging is less clear, there is mounting evidence that IIS regulates life span in mice (*1*). Global deletion of one allele of the IGF-1 receptor (*Igf1r*), adipose-specific deletion of the insulin receptor (*Insr*), global deletion of insulin receptor substrate protein 1 (*Irs1*), or neuron-specific deletion of *Irs2*, all increase mouse life span (*1*). Life-span–extending mutations in the somatotropic axis also appear to work through attenuated IIS (*3*). *Igf1r* has also been implicated as a modulator of human longevity (*4*). However, the action of downstream effectors of IIS or mTOR signaling in mammalian longevity is not fully understood.

S6K1 transduces anabolic signals that indicate nutritional status to regulate cell size and

[1]Institute of Healthy Ageing, Centre for Diabetes and Endocrinology, Department of Medicine, University College London, London WC1E 6JJ, UK. [2]Institute of Healthy Ageing, Department of Genetics, Evolution and Environment, University College London, London WC1E 6BT, UK. [3]European Bioinformatics Institute, Wellcome Trust Genome Campus, Hinxton, Cambridge CB10 1SD, UK. [4]Division of Molecular Neuroendocrinology, Medical Research Council National Institute for Medical Research, London NW7 1AA, UK. [5]Laboratory of Lymphocyte Signalling and Development, The Babraham Institute, Cambridge CB22 3AT, UK. [6]Cellular Stress Group, Medical Research Council Clinical Sciences Centre, Imperial College, London W12 0NN, UK. [7]Department of Cancer and Cell Biology, Genome Research Institute, University of Cincinnati, Cincinnati, OH 45237, USA. [8]Metabolic Signaling Group, Medical Research Council Clinical Sciences Centre, Imperial College, London W12 0NN, UK.

*Present address: Institute of Biological and Environmental Sciences, University of Aberdeen, Aberdeen AB24 2TZ, UK.
†To whom correspondence should be addressed. E-mail: d.withers@ucl.ac.uk or d.withers@imperial.ac.uk.

growth and metabolism through various mechanisms (*5*). These include effects on the translational machinery and on cellular energy levels through the activity of adenosine monophosphate (AMP)–activated protein kinase (AMPK) (*6*, *7*). Furthermore, S6K1 serine phosphorylates IRS1 and IRS2, which decreases insulin signaling (*5*). Given the key role of S6K1 in IIS and mTOR signaling and the regulation of aging in lower organisms by mTOR, S6K, and their downstream effectors (*2*), we used log-rank testing to evaluate differences in life span of wild-type (WT) and *S6K1*$^{-/-}$ littermate mice on a C57BL/6 background (*8*, *9*). Data for both sexes combined showed median life-span in *S6K1*$^{-/-}$ mice increased by 80 days (from 862 to 942 days) or 9% relative to that of WT mice ($\chi^2 = 10.52$, $P < 0.001$) (Fig. 1A and Table 1). Maximum life span (mean life span of the oldest 10% within a cohort) was also increased (1077 ± 16 and 1175 ± 24 days, $P < 0.01$ for WT and *S6K1*$^{-/-}$ mice, respectively). Analysis of each sex separately showed that median life span in female *S6K1*$^{-/-}$ mice was increased by 153 days (from 829 to 982 days) or 19% relative to that of WT mice ($\chi^2 = 11.07$, $P < 0.001$) (Fig. 1B and Table 1). Female maximum life-span was also increased (Table 1). In contrast, deletion of *S6K1* in male mice had no effect on median ($\chi^2 = 0.34$, $P > 0.05$) (Fig. 1C and Table 1) or maximum life span (Table 1). Similar gender effects on life span have been reported in other long-lived IIS mouse mutants (*8*, *10*). Cox regression analysis of pooled male and female lifespan data revealed no effect of recruitment date, parental identity, or gender, but that of genotype was significant (table S1). Therefore, deletion of *S6K1* increases longevity in female mice.

Female *S6K1*$^{-/-}$ mice also showed improvements in a number of age-sensitive biomarkers of aging. In forced motor activity on a rotating rod (rotarod) assays to assess motor and neurological function, 600-day-old female *S6K1*$^{-/-}$ mice performed better than WT littermates (Fig. 2A). Performance in open-field testing to analyze general activity and exploratory drive were also enhanced (Fig. 2, B and C). An increase in abundance of memory T cells and a reduced number of naïve T cells are seen in mice with age, and the extent of these changes may be correlated with longevity (*11*). Female *S6K1*$^{-/-}$ mice at 600 days of age had significantly fewer memory and more naïve T cells than did WT mice (Fig. 2D), although male mice also displayed this phenotype (fig. S1A). Micro–computed tomography scanning of tibia from 600-day-old female *S6K1*$^{-/-}$ mice revealed attenuation of the normal age-dependent loss of cancellous bone volume seen in C57BL/6 mice (*12*) (Fig. 2, E and F). However, there was no difference in the incidence of macroscopic tumors in *S6K1*$^{-/-}$ and WT animals [8% (4 out of 48) for *S6K1*$^{-/-}$ and 8% (4 out of 49) for WT mice, respectively].

Young, male *S6K1*$^{-/-}$ mice fed a high-fat diet (*13*) display increased insulin sensitivity and reduced adiposity relative to those of WT mice, phenotypes also seen in WT mice under caloric restriction (CR), an evolutionarily conserved environmental manipulation that extends life span (*14*). Insulin sensitivity (assessed by the updated homeostasis model, HOMA2) was significantly greater in 600-day-old female *S6K1*$^{-/-}$ mice than in WT animals (Fig. 2G), and glucose tolerance was improved (Fig. 2H), in contrast to the impaired glucose tolerance seen in young animals (fig S1B). Fat mass and plasma leptin levels were lower in old female *S6K1*$^{-/-}$ mice (Fig. 2, I and J), despite increased food intake (fig. S1C). Core temperature and resting metabolic rate (with general linear modeling to account for body-mass differences) were not significantly different (fig. S1, D and E). Although *S6K1*$^{-/-}$ mice were smaller than their littermates throughout their lives (Fig. 2K), endocrinologically they did not resemble long-lived pituitary dwarfs (*15*), because their total circulating IGF-1, pituitary growth hormone, thyroid-stimulating hormone, and prolactin concentrations were normal (Fig. 2, L and M, and fig. S1, F and G). Male *S6K1*$^{-/-}$ mice at 600 days of age had normal fasting and fed glucose levels (fig. S1, H and I).

We compared the effect of *S6K1* deletion on genome-wide hepatic gene expression in 600-day-old female mice to transcriptional changes induced by long-term CR (*16*). The 500 gene categories most overrepresented among genes with altered expression in *S6K1*$^{-/-}$ mice showed

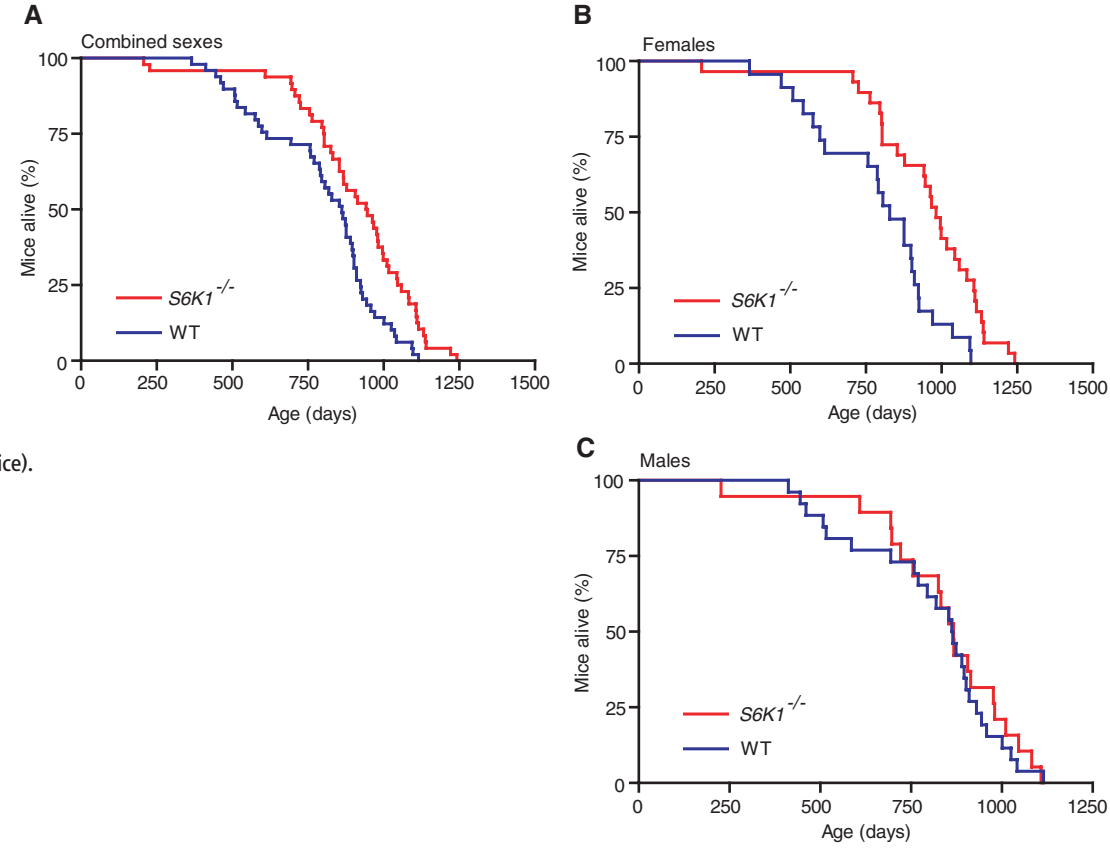

Fig. 1. Extended life span of mice with deletion of *S6K1*$^{-/-}$. (**A**) Kaplan-Meier survival curves for combined male and female wild-type (WT) and *S6K1*$^{-/-}$ mice show a significant (log-rank $\chi^2 = 10.52$, $P < 0.001$) life-span extension in *S6K1*$^{-/-}$ mice ($n = 49$ for WT mice and $n = 48$ for *S6K1*$^{-/-}$ mice). (**B**) Life-span extension was observed in female *S6K1*$^{-/-}$ mice ($\chi^2 = 11.07$, $P < 0.001$; $n = 23$ for WT mice and $n = 29$ for *S6K1*$^{-/-}$ mice). (**C**) No significant increase in life span in *S6K1*$^{-/-}$ mice ($\chi^2 = 0.34$, $P > 0.05$; $n = 26$ for WT mice and $n = 19$ for *S6K1*$^{-/-}$ mice).

a highly significant overlap with categories over-represented among CR-regulated genes ($P = 3.25 \times 10^{-42}$ and $P = 1.15 \times 10^{-19}$ for up- and down-regulated categories, respectively, Fisher's exact test) (fig. S2A). Hepatic transcript profiles in long-lived *Irs1*$^{-/-}$ mice (*8*) were also similar ($P = 1.60 \times 10^{-21}$ and $P = 8.61 \times 10^{-20}$ for up- and down-regulated categories, respectively) (fig. S2B). Furthermore, we observed significant correlations in the directions of transcriptional changes associated with highly significant functional categories ($P < 10^{-4}$, two-tailed) in both comparisons (fig. S2, A and B). This is consistent with the existence of common mechanisms underlying the effects of S6K1, CR, and IIS on aging.

We examined transcription of individual genes in liver, skeletal muscle, and white adipose tissue (WAT) in 600-day-old female *S6K1*$^{-/-}$ and WT mice, looking for genes previously associated with longevity (tables S2, A and B, S3, A and B, and S4, A and B). Significant cross talk exists between peroxisome proliferator–activated receptor (PPAR)–γ, coactivator 1 α (PGC-1α), AMPK, and nicotinamide adenine dinucleotide (oxidized form)–dependent deacetylase sirtuin-1 (SIRT1) signaling, which may be critical to cellular energy metabolism and perhaps aging (*17*). Increased expression of genes associated with these pathways was observed in liver (*Ppargc1a*, *Ppargc1b*, *Foxo1*, *Foxo3a*, *Cpt1b*, *Pdk4*, *Glut1*, *and Cyc*) and muscle (*Ppargc1a*, *Ppara*, *Foxo1*, *Foxo3a*, *Pdk4*, *Glut1*, *Sirt1*, *and Ucp3*) of *S6K1*$^{-/-}$ mice. Adipose tissue is a key tissue in longevity assurance in *C. elegans*, *D. melanogaster*, and mice (*18*). In WAT of *S6K1*$^{-/-}$ mice, fewer PGC-1α–regulated genes (*Foxo3a*, *Pdk4*, *Nampt*, and *Angptl4*) showed increased expression compared with changes seen in liver and muscle, but there was also increased expression of the α2 catalytic and β1 regulatory subunits of AMPK (log 2 fold change = 1.7, $P = 2.88 \times 10^{-6}$ and 1.2, $P = 4.95 \times 10^{-5}$, respectively, Cyber-T analysis). AMPK activity is increased in WAT, muscle, and liver of *S6K1*$^{-/-}$ mice (*7*). Moreover, comparison of gene expression patterns in muscle of *S6K1*$^{-/-}$ mice with those of mice treated with the AMPK activator aminoimidazole carboxamide ribo-

Table 1. Comparative survival characteristics of *S6K1*$^{-/-}$ and WT mice. Oldest (youngest) 10% are the mean life span of the longest (or shortest) living 10% of animals within a genotype. Values are reported ±SEM, where appropriate.

Genotype	Life span (days)					*n*
	Median	Mean	Min–Max	Oldest 10%	Youngest 10%	
			Combined sex			
WT	862	796 ± 28	365–1115	1077 ± 16	431 ± 19	49
***S6K1*$^{-/-}$**	942	907 ± 30	207–1242	1175 ± 24	487 ± 111	48
			Female			
WT	829	789 ± 42	365–1097	1096 ± 2	418 ± 53	23
***S6K1*$^{-/-}$**	982	950 ± 38	207–1242	1201 ± 31	546 ± 170	29
			Male			
WT	862	801 ± 39	412–1115	1061 ± 28	439 ± 14	26
***S6K1*$^{-/-}$**	867	841 ± 47	227–1108	1095 ± 13	418 ± 191	19

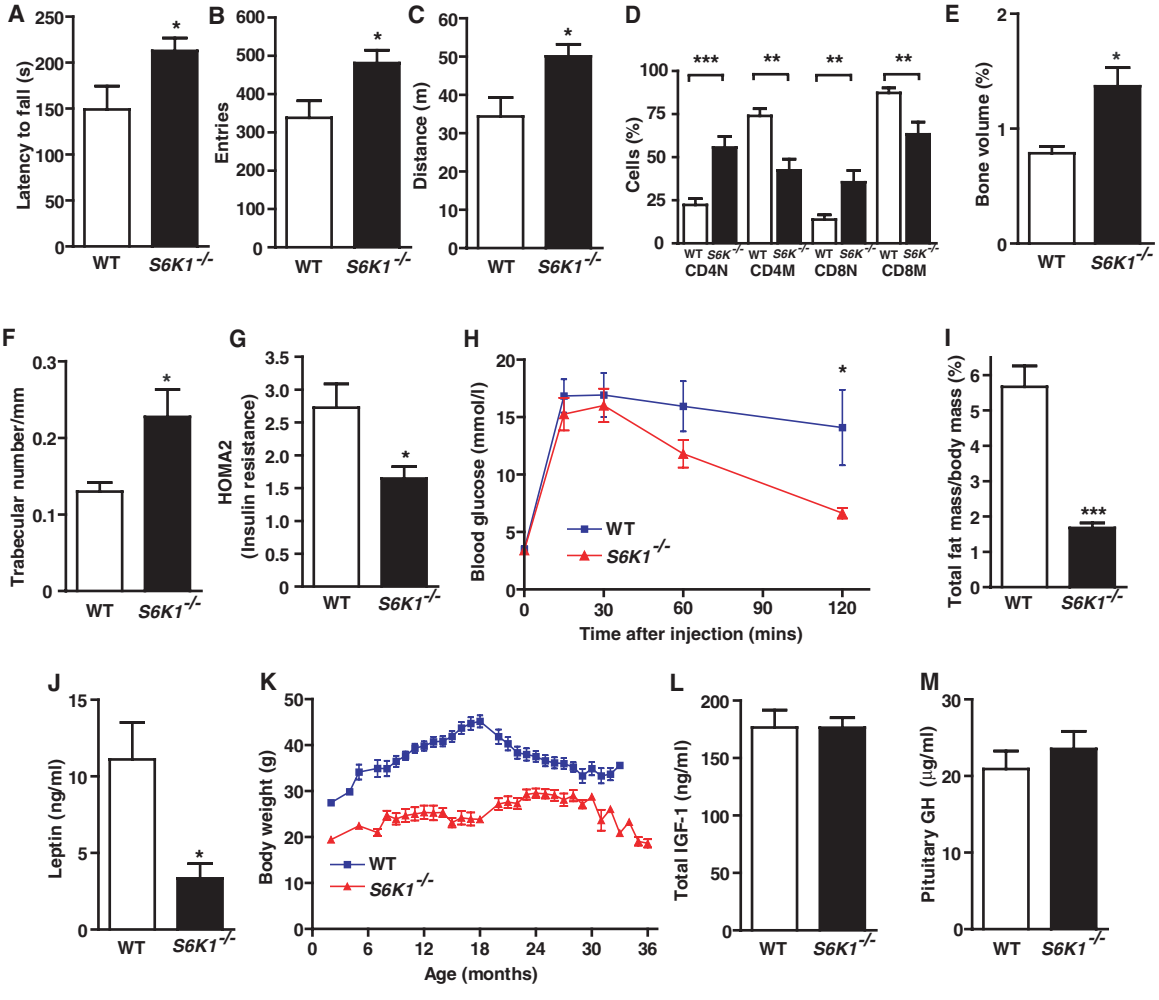

Fig. 2. Age-related pathology and physiological characteristics of 600-day-old female *S6K1*$^{-/-}$ mice. (**A**) *S6K1*$^{-/-}$ mice had improved rotarod performance. (**B** and **C**) Increased general activity and exploratory drive was observed in *S6K1*$^{-/-}$ mice. (**D**) Abundance of memory and naïve T cells in WT and *S6K1*$^{-/-}$ mice. (**E** and **F**) Bone volume and trabecular number in WT and *S6K1*$^{-/-}$ mice. (**G** and **H**) Insulin sensitivity and glucose tolerance of WT and *S6K1*$^{-/-}$ mice. (**I**) *S6K1*$^{-/-}$ mice were lean and (**J**) had reduced plasma leptin levels. (**K**) Body mass ($P < 0.01$ at all time points), total circulating IGF-1 (**L**), and pituitary growth hormone (GH) concentrations in WT and *S6K1*$^{-/-}$ mice (**M**). Values are means ±SEM. Asterisks indicate statistical difference compared with WT mice by using two-tailed *t* tests, *$P < 0.05$; **$P < 0.01$; and ***$P < 0.001$; $n = 6$ to 8 per genotype.

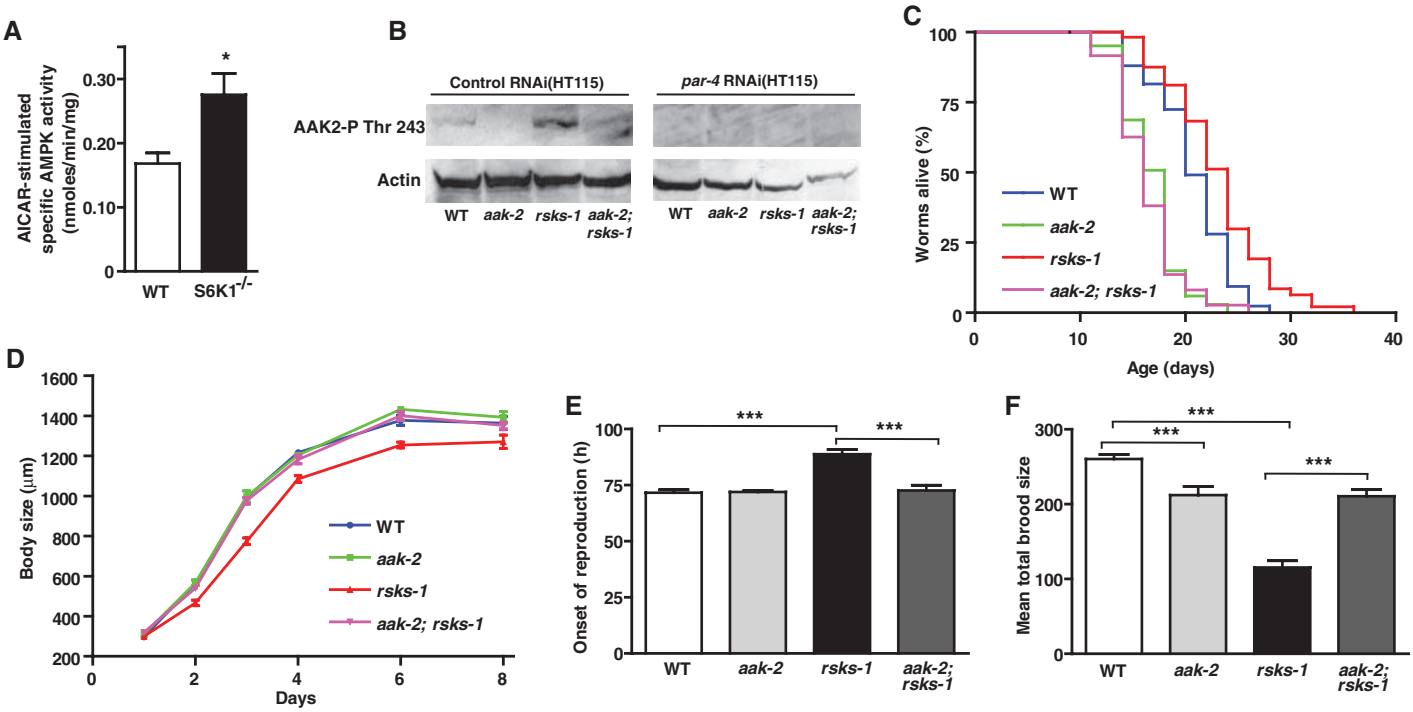

Fig. 3. Enhanced AMPK activation by AICAR of *S6K1*$^{-/-}$ hepatocytes, increased AAK-2 phosphorylation in *rsks-1(ok1255)* mutants, and effects of loss of *aak-2(ok524)* on longevity and physiology. (**A**) AICAR-stimulated AMPKα2 activity in isolated hepatocytes from *S6K1*$^{-/-}$ mice. (**B**) Phosphorylation of AAK-2 Thr^{243} in *rsks-1(ok1255)* null mutants subjected, or not, to RNA interference for *par-4*, the worm LKB kinase that effects this phosphorylation. (**C**) Life span of *rsks-1(ok1255)* nulls with mutation of *aak-2(ok524)*. (**D** to **F**) Body length, onset of reproductive function, and brood-size phenotypes in *rsks-1(ok1255)* mutants with or without *aak-2(ok524)* mutation. In (D), *rsks-1(ok1255)* is significantly different ($P < 0.001$; one-way ANOVA) from all other groups from day 2 onward, but *rsks-1(ok1255);aak-2* is not significantly different from WT or *aak-2*. (A) to (C) show data from one representative experiment, and (D to F) show combined data from three similar independent experiments. Values (A and D to F) are means ±SEM. In (A), $n = 3$, and in (D), $n > 8$ for each strain and time point. For (E) and (F), $n > 20$ for each group. Asterisks indicate statistical differences by using two-tailed *t* tests, $^{*}P < 0.05$, $^{***}P < 0.001$.

nucleotide (AICAR) (*19*) revealed a strong overlap between gene categories that showed increased expression, including those associated with PPAR signaling and lipid metabolism (fig. S2C). We confirmed enhanced AMPK activation by AICAR in isolated hepatocytes from *S6K1*$^{-/-}$ mice (Fig. 3A).

In *C. elegans*, AMPK mediates the effects on life-span of one particular form of CR (*20*) and perturbing IIS (*21*, *22*), which raises the possibility that the longevity of *S6K1*$^{-/-}$ mice results from increased AMPK activity. To test this, we studied long-lived *C. elegans rsks-1(ok1255)* null mutants, which lack the single worm S6K1 homolog. *rsks-1* mutants showed increased phosphorylation of the worm AMPK catalytic subunit AAK-2 (Fig. 3B), consistent with increased AMPK activity. These findings imply that in worms, as in mice, loss of S6K1 increases AMPK activity. *rsks-1* mutants are long-lived (Fig. 3C, and table S5), with reduced and delayed fecundity and, like *S6K1*$^{-/-}$ mice, reduced body size (Fig. 3, D to F, and table S5), characteristics that could be attributed to reduced nutrient availability or possibly reduced overall translation (*23*). To test the role of AMPK in mediating the effects of *rsks-1* on longevity, we generated mutants lacking both *rsks-1* and *aak-2*. The *aak-2(ok524)* null allele fully suppressed *rsks-1* mutant longevity (Fig. 3C, and table S5). This effect is likely to be specific, because several other modes of *C. elegans* longevity are not *aak-2*–dependent (*22*). Moreover, *aak-2(ok524)* also suppressed the fecundity and body size defects of *rsks-1* mutants (Fig. 3, D to F). This also suggests that these defects do not reflect reduced overall translation; in fact, in muscle cells from growth-deficient *S6K1* null mice, protein synthesis is reportedly not reduced (*24*). Taken together, these results imply that increased AMPK activity may contribute to the longevity of both *C. elegans* and mice lacking *S6K1*.

Our studies indicate that S6K1 signaling influences mammalian life span and age-related pathology. S6K1 is regulated in response to nutrient and hormonal signals and may thus participate in the response to CR. mTOR and AMPK are amenable to pharmacological intervention (*25*, *26*). It might be possible to develop drug treatments that manipulate S6K1 and AMPK to achieve improved overall health in later life. Indeed, short-term rapamycin treatment reduces adiposity in mice (*27*), and metformin treatment extends life span in short-lived mice (*28*). Furthermore, recently it has been demonstrated that rapamycin treatment initiated late in life extends life span in mice (*29*). Our results suggest that this may occur via inhibition of S6K1, and together, these studies indicate the feasibility of manipulating mTOR/S6K1 signaling in the treatment of aging-related disease.

References and Notes

1. M. D. Piper, C. Selman, J. J. McElwee, L. Partridge, *J. Intern. Med.* **263**, 179 (2008).
2. M. N. Stanfel, L. S. Shamieh, M. Kaeberlein, B. K. Kennedy, *Biochim. Biophys. Acta*, 10.1016/j.bbagen.2009.06.007, published online 16 June 2009.
3. M. M. Masternak, J. A. Panici, M. S. Bonkowski, L. F. Hughes, A. Bartke, *J. Gerontol. A Biol. Sci. Med. Sci.* **64**, 516 (2009).
4. Y. Suh *et al.*, *Proc. Natl. Acad. Sci. U.S.A.* **105**, 3438 (2008).
5. S. H. Um, D. D'Alessio, G. Thomas, *Cell Metab.* **3**, 393 (2006).
6. P. Gulati, G. Thomas, *Biochem. Soc. Trans.* **35**, 236 (2007).
7. V. Aguilar *et al.*, *Cell Metab.* **5**, 476 (2007).
8. C. Selman *et al.*, *FASEB J.* **22**, 807 (2008).
9. Materials and methods are available as supporting material on *Science* Online.
10. M. Holzenberger *et al.*, *Nature* **421**, 182 (2003).
11. R. A. Miller, *J. Gerontol. A Biol. Sci. Med. Sci.* **56**, B180 (2001).
12. B. P. Halloran *et al.*, *J. Bone Miner. Res.* **17**, 1044 (2002).
13. S. H. Um *et al.*, *Nature* **431**, 200 (2004).
14. W. Mair, A. Dillin, *Annu. Rev. Biochem.* **77**, 727 (2008).
15. A. Bartke, *Aging Cell* **7**, 285 (2008).
16. J. M. Dhahbi, H. J. Kim, P. L. Mote, R. J. Beaver, S. R. Spindler, *Proc. Natl. Acad. Sci. U.S.A.* **101**, 5524 (2004).
17. C. Canto *et al.*, *Nature* **458**, 1056 (2009).
18. F. Picard, L. Guarente, *Int. J. Obes. (London)* **29** (suppl. 1), S36 (2005).
19. V. A. Narkar *et al.*, *Cell* **134**, 405 (2008).
20. E. L. Greer *et al.*, *Curr. Biol.* **17**, 1646 (2007).
21. J. Apfeld, G. O'Connor, T. McDonagh, P. S. DiStefano, R. Curtis, *Genes Dev.* **18**, 3004 (2004).

22. R. Curtis, G. O'Connor, P. S. DiStefano, *Aging Cell* **5**, 119 (2006).
23. K. Z. Pan *et al.*, *Aging Cell* **6**, 111 (2007).
24. V. Mieulet *et al.*, *Am. J. Physiol. Cell Physiol.* **293**, C712 (2007).
25. D. A. Guertin, D. M. Sabatini, *Sci. Signal.* **2**, pe24 (2009).
26. B. B. Zhang, G. Zhou, C. Li, *Cell Metab.* **9**, 407 (2009).
27. G. R. Chang *et al.*, *J. Pharmacol. Sci.* **109**, 496 (2009).
28. V. N. Anisimov *et al.*, *Cell Cycle* **7**, 2769 (2008).
29. D. E. Harrison *et al.*, *Nature* **460**, 392 (2009).

30. Supported by a Wellcome Trust Functional Genomics award to J.M.T., L.P., D.G., and D.J.W.; a Wellcome Trust Strategic Award to J.M.T., L.P., D.G., and D.J.W.; and grants from the Medical Research Council, Research into Aging, and the Biological and Biotechnology Research Council to D.J.W.

Supporting Online Material
www.sciencemag.org/cgi/content/full/326/5949/140/DC1
Materials and Methods
Figs. S1 and S2
Tables S1 to S5
References

3 June 2009; accepted 24 August 2009
10.1126/science.1177221

Genome-Wide RNAi Screen Identifies Letm1 as a Mitochondrial Ca^{2+}/H^{+} Antiporter

Dawei Jiang, Linlin Zhao, David E. Clapham*

Mitochondria are integral components of cellular calcium (Ca^{2+}) signaling. Calcium stimulates mitochondrial adenosine 5′-triphosphate production, but can also initiate apoptosis. In turn, cytoplasmic Ca^{2+} concentrations are regulated by mitochondria. Although several transporter and ion-channel mechanisms have been measured in mitochondria, the molecules that govern Ca^{2+} movement across the inner mitochondrial membrane are unknown. We searched for genes that regulate mitochondrial Ca^{2+} and H^{+} concentrations using a genome-wide *Drosophila* RNA interference (RNAi) screen. The mammalian homolog of one *Drosophila* gene identified in the screen, *Letm1*, was found to specifically mediate coupled Ca^{2+}/H^{+} exchange. RNAi knockdown, overexpression, and liposome reconstitution of the purified Letm1 protein demonstrate that Letm1 is a mitochondrial Ca^{2+}/H^{+} antiporter.

Mitochondrial Ca^{2+} uptake across the inner mitochondrial membrane occurs via tightly regulated channels [e.g., MCU/MiCa (*1*, *2*) and transporters (*3*–*6*)]. Increases in the concentration of calcium ($[Ca^{2+}]$) in the mitochondrial matrix enhance the activities of adenosine 5′-triphosphate (ATP) synthase and enzymes in the tricarboxylic acid cycle (*7*, *8*), but if homeostatic mechanisms fail, high levels of matrix Ca^{2+} induce cell death (*9*, *10*). We set out to identify the genes that mediate Ca^{2+} flux across the inner mitochondrial membrane.

We conducted a genome-wide, high-throughput RNA interference (RNAi) screen to identify genes that control mitochondrial Ca^{2+} transport. *Drosophila* S2 cells stably expressing mitochondria-targeted ratiometric pericam were incubated with arrayed double-stranded RNAs (dsRNAs) against each of the ~22,000 *Drosophila* genes (*11*). Mitochondrial (Mt)-pericam emission due to excitation at 405 nm is sensitive to changes in $[Ca^{2+}]$, whereas emission in response to excitation at 488 nm independently reports changes in pH (figs. S1 and S2). Through a series of screens discussed in the supporting online material (SOM) (fig. S2 and tables S1 to S3), *CG4589*, the *Drosophila* homolog of the human gene *Letm1*, was identified as a gene strongly affecting $[Ca^{2+}]_{mito}$ and $[H^{+}]_{mito}$

Department of Cardiology, Howard Hughes Medical Institute, Children's Hospital Boston, Manton Center for Orphan Disease, and Department of Neurobiology, Harvard Medical School, Enders Building 1309, 320 Longwood Avenue, Boston, MA 02115, USA.

*To whom correspondence should be addressed. E-mail: dclapham@enders.tch.harvard.edu

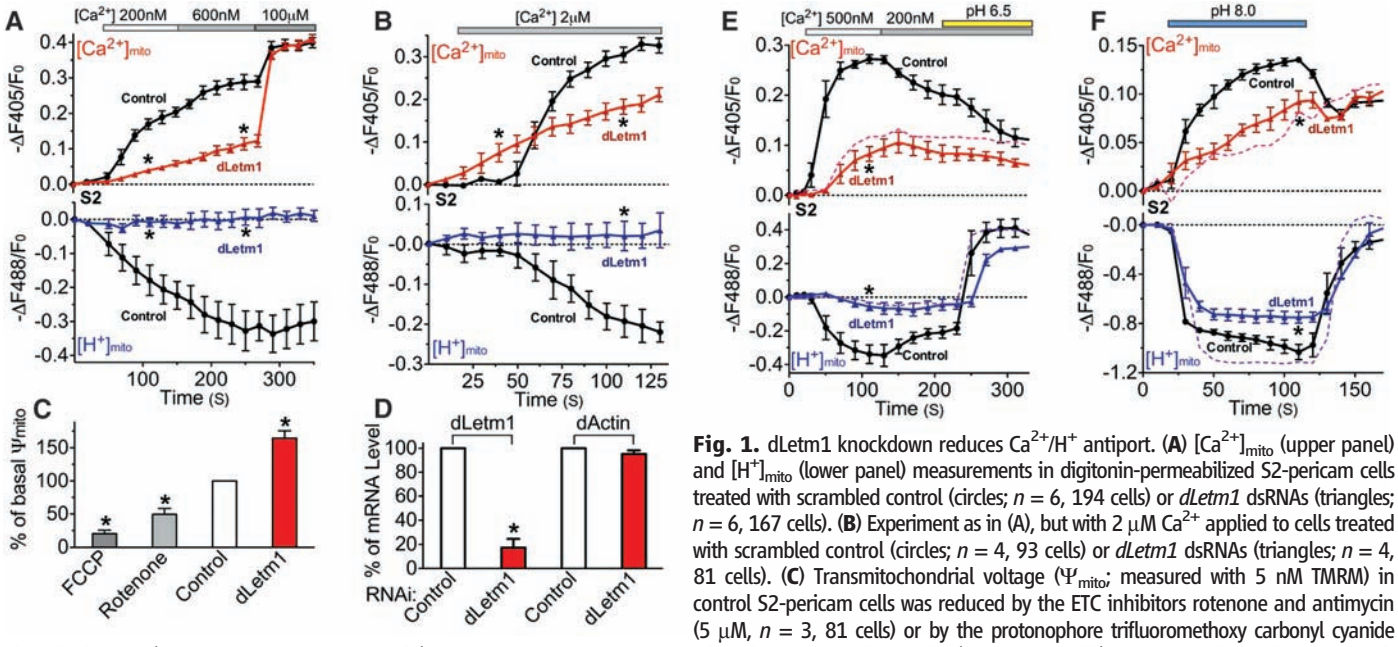

Fig. 1. dLetm1 knockdown reduces Ca^{2+}/H^{+} antiport. (**A**) $[Ca^{2+}]_{mito}$ (upper panel) and $[H^{+}]_{mito}$ (lower panel) measurements in digitonin-permeabilized S2-pericam cells treated with scrambled control (circles; $n = 6$, 194 cells) or *dLetm1* dsRNAs (triangles; $n = 6$, 167 cells). (**B**) Experiment as in (A), but with 2 μM Ca^{2+} applied to cells treated with scrambled control (circles; $n = 4$, 93 cells) or *dLetm1* dsRNAs (triangles; $n = 4$, 81 cells). (**C**) Transmitochondrial voltage (Ψ_{mito}; measured with 5 nM TMRM) in control S2-pericam cells was reduced by the ETC inhibitors rotenone and antimycin (5 μM, $n = 3$, 81 cells) or by the protonophore trifluoromethoxy carbonyl cyanide phenylhydrazone (FCCP; 10 μM, $n = 3$, 102 cells). By contrast, Ψ_{mito} was increased in dLetm1 knockdown cells ($n = 3$, 113 cells) as compared to cells treated with scrambled control dsRNA ($n = 3$, 168 cells). (**D**) Relative mRNA level of dLetm1 and actin in control and *dLetm1* dsRNA-treated S2 cells by quantitative reverse transcription–polymerase chain reaction (RT-PCR) ($n = 3$). (**E**) Ca^{2+}- and pH gradient–driven $[Ca^{2+}]_{mito}$ and $[H^{+}]_{mito}$ changes in permeabilized S2-pericam cells treated with control (circles; $n = 4$, 143 cells) or *dLetm1* dsRNAs (triangles; $n = 4$, 113 cells). A representative trace shows the effect of applying the H^{+}/K^{+} antiporter nigericin (1 μM, dashed colored line) on *dLetm1* dsRNA-treated cells ($n = 3$, 87 cells). (**F**) pH-dependent $[Ca^{2+}]_{mito}$ and $[H^{+}]_{mito}$ changes in permeabilized S2-pericam cells treated with scrambled control (circles; $n = 6$, 214 cells) or *dLetm1* dsRNAs (triangles; $n = 6$, 187 cells). BAPTA-maintained test solution $[Ca^{2+}] = 50$ nM. A representative trace shows the effect of nigericin (1 μM, dotted line) on *dLetm1* dsRNA-treated cells ($n = 3$, 104 cells). All data shown are the mean ± SEM (*$P < 0.05$, two-tailed Student's *t* test).